

Chao Qiu<sup>1</sup>  
Hui Xu<sup>1,\*</sup>

## A Six-Gene Signature Related to Liquid-Liquid Phase Separation for Diagnosis of Alzheimer's Disease

<sup>1</sup>Department of Neurology, The First Affiliated Hospital of Zhejiang Chinese Medical University (Zhejiang Provincial Hospital of Chinese Medicine), 310006 Hangzhou, Zhejiang, China

### Abstract

**Background:** Liquid-liquid phase separation (LLPS) has been increasingly recognized as a crucial mechanism in the pathogenesis of various neurodegenerative disorders, including Alzheimer's disease (AD). There remains a paucity of effective diagnostic biomarkers for this condition. This study aims to develop and validate a novel LLPS-related molecular signature to enhance the diagnostic accuracy and early detection of AD.

**Methods:** LLPS-related genes were identified from online databases and subjected to bioinformatic analyses, including protein-protein interaction (PPI) network analysis and least absolute shrinkage and selection operator (LASSO) regression. Based on the optimal LLPS-related genes, a diagnosis risk model was constructed, and the diagnostic ability was evaluated using a receiver operator characteristic (ROC) curve. To elucidate the biological functions of the identified LLPS-related genes, Gene Ontology (GO) and Kyoto Encyclopedia of Genes and Genomes (KEGG) analyses were conducted.

**Results:** A total of 149 LLPS-related genes were screened, which were found to be involved in functions related to oxidative stress, apoptosis, and cancer progression. The 149 genes were refined to six optimal candidates through PPI network analysis and LASSO regression: Activator of HSP90 ATPase Activity 1 (*AHS1*), Eukaryotic Translation Initiation Factor 2 Alpha Kinase 2 (*EIF2AK2*), Heat Shock Protein Family A (Hsp70) Member 4 (*HSPA4*), Notch Receptor 1 (*NOTCH1*), Superoxide Dis-

mutase 1 (*SOD1*), and Thioredoxin (*TXN*). Based on the six optimal genes, a diagnostic risk model was constructed, and the diagnostic ability was verified to be promising in AD both in training, internal validation, and two external validation datasets, with area under ROC curve (AUC) above 0.8. Furthermore, significant correlations were observed between the expression of these genes and tumor immune cell infiltration.

**Conclusions:** A six-gene diagnosis model was constructed and verified to exhibit robust diagnostic ability in AD.

### Keywords

Alzheimer's disease; diagnosis; liquid-liquid phase separation; immune microenvironment

### Introduction

Alzheimer's disease (AD) is the most prevalent form of dementia and has emerged as one of the most lethal diseases [1,2]. The incidence of AD is increasing, and the most recent study indicates that the prevalence of dementia is expected to double in Europe and triple globally by 2050 [3]. Patients diagnosed with AD typically face poor prognosis, with a median survival time ranging from 5 to 10 years post-diagnosis [4]. Despite the approval of several pharmacological drugs by the Food and Drug Administration to mitigate AD progression [5], the efficacy of these treatments remains limited, largely due to the heterogeneous nature of the disease [6]. The absence of early diagnostic tools and effective therapeutic strategies for AD underscores the critical need for further exploration of precise molecular markers characteristic of this neurodegenerative disorder.

The diagnosis of AD is primarily based on clinical symptomatology, although pathological changes typically

\*Corresponding author details: Hui Xu, Department of Neurology, The First Affiliated Hospital of Zhejiang Chinese Medical University (Zhejiang Provincial Hospital of Chinese Medicine), 310006 Hangzhou, Zhejiang, China. Email: 13989873337@163.com

precede the onset of overt symptoms. Amyloid- $\beta$  and tau deposition can occur before clinical manifestations, a fact that has been incorporated into diagnostic criteria for asymptomatic individuals [7]. The liquid-liquid phase separation (LLPS) theory has gained prominence in explaining multiple cellular biological processes, including DNA damage repair, transcription regulation, and protein degradation. Recent research by Liu *et al.* [8] has elucidated the role of LLPS inhibition in hepatocellular carcinoma metastasis. Their findings demonstrate that circRNA-Y-box binding protein 1 (YBX1)-mediated phase separation influences cytoskeleton remodeling, thereby modulating the metastatic potential of hepatocellular carcinoma cells. LLPS has also been demonstrated to have close interconnections with the pathogenesis of various neurodegenerative disorders, including AD, which is characterized by the deposition and generation of amyloid- $\beta$  and tau proteins [9]. Wegmann *et al.* [10] demonstrated that intracellular tau LLPS induces the formation of subcellular foci with high local concentrations of tau in AD. Additionally, heparin has been found to interact with tau and facilitate its LLPS in AD [11]. This evidence indicates that LLPS is significantly correlated with AD progression and may potentially serve as a diagnostic signature for the disease.

Previous research has reported clinical, mitophagy, and ferroptosis signatures in AD diagnosis and prognosis [12–14]. However, limited research has focused on LLPS-related gene signatures in AD. This study aimed to identify an LLPS-related diagnostic gene signature for AD patients using bioinformatic approaches. A six-gene diagnostic model was subsequently established. Additionally, the correlations between these six key genes and immune cell populations were investigated to elucidate potential immunological implications.

## Materials and Methods

### Data Source

The peripheral blood sample dataset GSE63060 was downloaded from the Gene Expression Omnibus (GEO) database (<https://www.ncbi.nlm.nih.gov/geo/>) as the training dataset, comprising 145 disease samples and 104 normal blood samples. For external validation, datasets GSE1297 and GSE63061 were also obtained. GSE1297 included 22 disease and 9 normal tissue samples, while GSE63061 contained 139 disease and 134 normal blood samples.

AD-related genes were retrieved from the Comparative Toxicogenomics Database (CTD) (<https://ctdb>

[ase.org/](https://www.disgenet.org/)), DisGeNET (<https://www.disgenet.org/>), and GeneCards (<https://www.genecards.org/>) databases using “Alzheimer's Disease” as the key word.

LLPS-related genes were downloaded from the phasepdbv2 database (<http://db.phasep.pro/>), resulting in a total of 3775 LLPS-related genes.

### Differential Analysis

Differential gene expression analysis was conducted using the limma package (version 3.58.1, <http://www.bioconductor.org/packages/release/bioc/html/limma.html>, Walter and Eliza Hall Institute of Medical Research, Melbourne, Australia) [15] in R software to identify differentially expressed genes (DEGs) between AD and control samples from the GSE63060 dataset. The significance threshold was set at  $p < 0.05$  and  $|\log_2 \text{fold change (FC)}| > 0.1$ . Visualization of the analysis results was performed using the ggplot2 package (version 3.5.1, <https://ggplot2.tidyverse.org/articles/ggplot2.html>, Hadley Wickham, New Zealand) [16] in R.

### Venn and Functional Analysis

To identify genes associated with LLPS in AD, we performed a Venn analysis to intersect DEGs, AD-related genes, and LLPS-related genes. Gene Ontology (GO) and Kyoto Encyclopedia of Genes and Genomes (KEGG) pathway analyses were conducted using the clusterProfiler package (version 4.10.1, <https://www.bioconductor.org/packages/release/bioc/html/clusterProfiler.html>, Guangchuang Yu, Southern Medical University, Guangzhou, China) [17] in R, with a significance threshold of  $p < 0.05$ . For visualization, we displayed the top 15 enriched pathways if the total number of significant pathways exceeded 15; otherwise, all significant pathways were presented.

### Unsupervised Cluster Analysis

To investigate the links between overlapping genes and AD, we performed subtype analysis using ConsensusClusterPlus (version 1.66.0, <https://www.bioconductor.org/packages/release/bioc/html/clusterProfiler.html>, Guangchuang Yu, Southern Medical University, Guangzhou, China) [18]. This analysis was based on the previously identified overlapping genes. The Partitioning Around Medoids (PAM) algorithm was employed, with distance quantified using a “1-Pearson” correlation coefficient. We conducted 100 repetitions, exploring

cluster numbers ( $k$ ) ranging from 2 to 10. The optimal number of clusters ( $k = 2$ ) was determined through the evaluation of the cumulative distribution function (CDF).

Single-sample Gene Set Enrichment Analysis (ssGSEA), an extension of the Gene Set Enrichment Analysis (GSEA) method, is widely used in bioinformatics research to assess immune infiltration. The GSVA package (version 1.50.1, <https://www.bioconductor.org/packages/release/bioc/html/GSVA.html>, Robert Castelo, Universitat Pompeu Fabra (UPF), Barcelona, Spain) [19] was used to calculate enrichment scores of 19 distinct immune cell types across all samples. Immune cell markers were obtained from the CellMarker and previous publications. Subsequently, the ssGSEA method was applied to these markers to evaluate the immunoactivity score of each immune cell type, serving as a proxy for infiltration levels. Additionally, differences in leukocyte antigens between immune subtypes were examined using Student's  $t$ -test.

#### *Protein-Protein Interaction (PPI) Networks*

The STRING database (<https://cn.string-db.org/>) is a database of known and predicted PPIs. Interactions include direct (physical) and indirect (functional) connections; they arise from the interactions of computational prediction, knowledge transfer between organisms, and other (major) database aggregation. PPI networks of overlapping genes were constructed by STRIND database [20]. An interaction relationship greater than 0.4 was preserved. The core genes that were related to LLPS in AD in the PPI network were screened based on plug-in Mcode (version 1.4.2, <http://apps.cytoscape.org/apps/MCODE>, University of Toronto, Toronto, Canada). Cytoscape software (version 3.9.1, <http://www.cytoscape.org>, National Institute of General Medical Sciences, Bethesda, MD, USA) was used to visualize the PPI network.

#### *Least Absolute Shrinkage and Selection Operator (LASSO) Analysis*

LASSO regression is characterized by variable screening and complexity adjustment while fitting the generalized linear model. Based on the core genes from the PPI network, LASSO analysis was conducted to optimize the gene combination using the binomial method in the glmnet package (version 4.1-8, <https://glmnet.stanford.edu/articles/glmnet.html>, Trevor Hastie, Stanford University, Palo Alto, CA, USA) [21] in R. A diagnosis risk score model was established based on the expression levels and coefficients of genes selected through LASSO analysis. The AD

samples in the GSE63060 training dataset were randomly divided into training and validation subsets at a ratio of 1:1, with the latter serving as an internal validation set. The predictive performance of the risk score model was evaluated using Kaplan-Meier survival analysis and receiver operator characteristic (ROC) curve. All results were subsequently validated using both internal and external validation datasets. Finally, the expression levels of the key genes were further validated using the GSE63061 blood dataset.

#### *Correlation Analysis*

Pearson correlation coefficient analysis, a commonly used statistical method, was utilized to measure the strength and direction of linear associations between two variables. In our study, Pearson correlation coefficients were calculated using diagnostic model genes and the abundance of differentially represented immune cell populations.

#### *Statistical Analysis*

The statistical analyses were conducted using R software version 4.3.2 (R Foundation for Statistical Computing, Vienna, Austria). Statistical significance was set at  $p < 0.05$ . Wilcoxon and Student's  $t$ -tests were used to investigate the differences between two groups. Pearson and spearman methods were used to investigate the correlation between variables.

The study workflow is shown in Fig. 1.

## **Results**

#### *Differential Expression Analysis*

The analysis identified 2338 DEGs associated with AD, comprising 1123 upregulated and 1215 downregulated genes in AD samples (Fig. 2A). The intersection of DEGs, AD-related genes, and LLPS-related genes yielded 149 overlapping genes implicated in both LLPS and AD pathology (Fig. 2B). The functional analysis indicated that the 149 genes were involved into 725 biological processes (BPs), 61 molecular functions (MFs), 76 cellular components (CC), and 27 KEGG pathways. The top 15 enriched terms for each category are presented in Fig. 2C–F. Notably, the identified genes were associated with functions related to oxidative stress, apoptosis, and cancer progression.

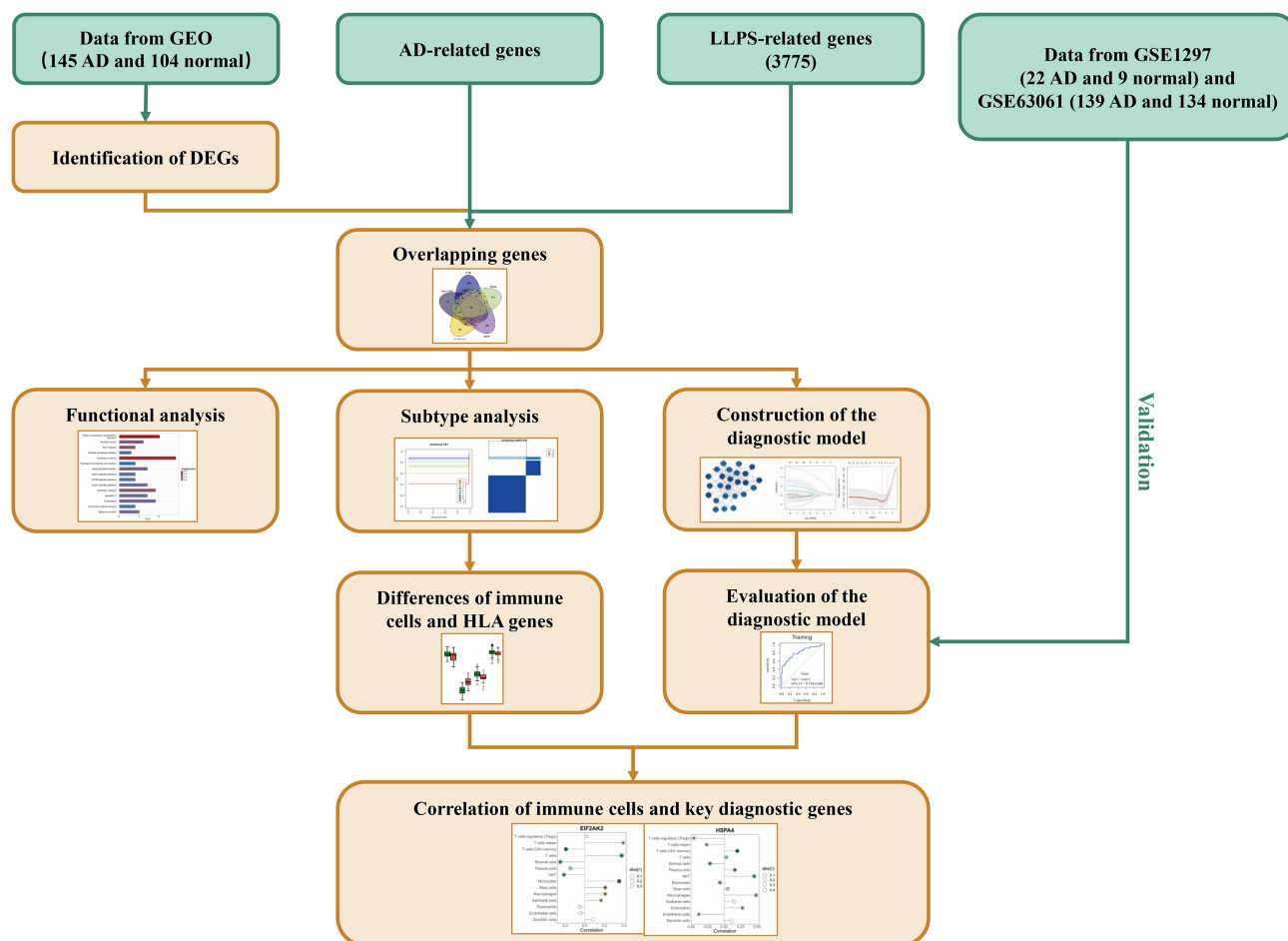


**Fig. 1. Study design.** GEO, Gene Expression Omnibus; AD, Alzheimer's disease; LLPS, liquid-liquid phase separation; HLA, human leukocyte antigen; DEGs, differential expressed genes. The picture is drawn in Microsoft PowerPoint 2021 (Microsoft. com, Redmond, WA, USA).

### Differential Subtypes

Based on the 149 overlapping genes, subtype analysis divided the AD samples into two distinct subtypes: subtype 1 and subtype 2 (Fig. 3A). Significant differences in the distribution of 14 immune cell types were observed between the two subtypes ( $p < 0.05$ ) (Fig. 3B). Notably, macrophages, memory T-Cell Surface Glycoprotein CD4 (CD4) T cells, and natural killer cell (NKT) exhibited significantly higher levels in subtype 2 compared to subtype 1 ( $p < 0.05$ ). Given the recent breakthroughs in cancer immunotherapy and the importance of human leukocyte antigens (HLAs) as indicators of immunotherapy, we examined the expression of 28 HLA genes across the two subtypes. Our analysis revealed significant differences in nine HLA genes between the two subtypes ( $p < 0.05$ ) (Fig. 3C). Specifically, HLA-Major Histocompatibility Complex Class II DR Alpha (DRA) and HLA-Major Histocompatibility Complex Class II DM Beta (DMB) were

significantly higher in subtype 2 relative to subtype 1 ( $p < 0.05$ ). Conversely, HLA-F, HLA-H, HHLA3, HLA-E, HLA-A, HLA-C, and HLA-B were significantly lower in subtype 2 compared to subtype 1 ( $p < 0.05$ ).

### Identification of Diagnosis Genes and Construction of Diagnosis Risk Score Model

To further screen the important LLPS genes in AD, PPI network analysis and LASSO regression were conducted. The PPI network analysis revealed 1278 interaction pairs (Fig. 4A), indicating a close relationship among these genes. Subsequently, through Molecular Complex Detection (MCODE) plugin analysis, 23 core genes were identified for further investigation (Fig. 4B). LASSO regression analysis was used to optimize the 23 core genes, resulting in the selection of six genes based on AD data from the training dataset (Fig. 4C). The diagnostic risk model was

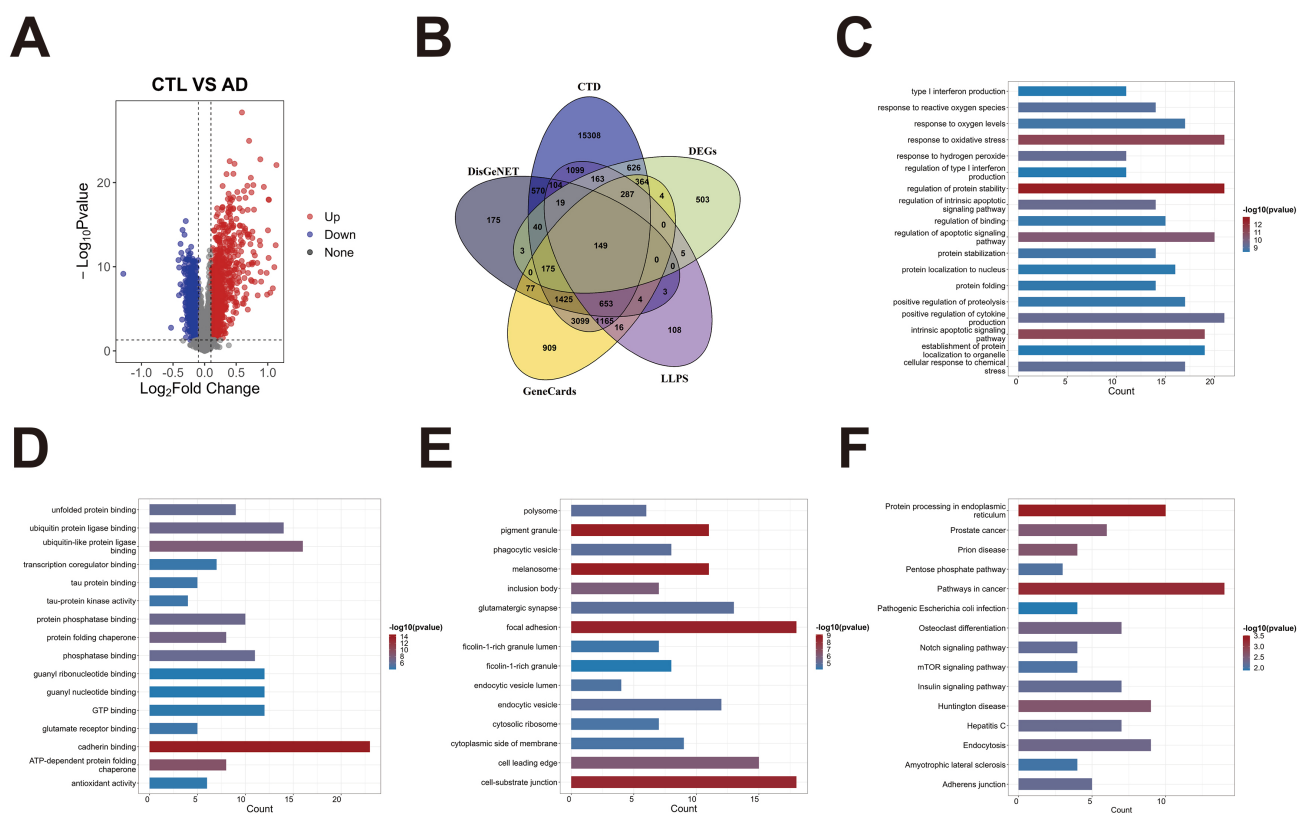


**Fig. 2. Identification of the LLPS-related genes.** (A) Volcano plot for selection of differential expressed genes (DEGs) between AD and normal samples. (B) Venn plot for selection of LLPS-related genes and 149 genes. (C) Gene Ontology (GO) biological process analysis for the 149 genes. (D) GO molecular function (MF) for the 149 genes. (E) GO cellular component for the 149 genes. (F) Kyoto Encyclopedia of Genes and Genomes (KEGG) pathways for the 149 genes. LLPS, liquid-liquid phase separation; CTD, Comparative Toxicogenomics Database.

established as follows: Risk score = 0.216 × Superoxide Dismutase 1 (*SOD1*) – 0.014 × Eukaryotic Translation Initiation Factor 2 Alpha Kinase 2 (*EIF2AK2*) + 3.446 × Activator of HSP90 ATPase Activity 1 (*AHS1*) + 0.706 × Thioredoxin (*TXN*) + 0.825 × Heat Shock Protein Family A (Hsp70) Member 4 (*HSPA4*) + 0.130 × Notch Receptor 1 (*NOTCH1*). ROC analysis showed that the diagnosis of the model was promising, with an area under ROC curve (AUC) of 0.808 (Fig. 4D). Moreover, the diagnostic efficacy of the risk score model was further validated through an internal and two external datasets, with an AUC above 0.7 (Fig. 4E,F). These results demonstrate that the constructed diagnostic risk model exhibited robust discriminatory power for AD patients across both training and validation datasets. To further validate the expression levels of the six identified genes, their expression levels were examined in two external blood sample datasets, GSE63060 and GSE63061. The results showed that five of the genes were significantly different between AD and normal groups in the both datasets (Fig. 4G).

### Correlation of Key Genes with Immune Cells

The correlations between the six diagnostic genes incorporated in the diagnostic model and the 14 differentially expressed immune cells across subtypes were investigated (Fig. 5A–F), revealing significant associations. Specifically, *HSPA4*, *SOD1*, and *TXN* exhibited negative correlations with Tregs, while *NOTCH1* demonstrated a positive correlation. *EIF2AK2* and *NOTCH1* showed negative correlations with CD4 memory T cells, while *HSPA4*, *SOD1*, and *TXN* displayed positive correlations. *EIF2AK2* and *NOTCH1* were negatively correlated with NKT, while *SOD1* and *TXN* were positively correlated with NKT. *EIF2AK2*, *HSPA4*, *SOD1*, and *TXN* exhibited positive correlations with macrophages, while *NOTCH1* demonstrated a negative correlation.

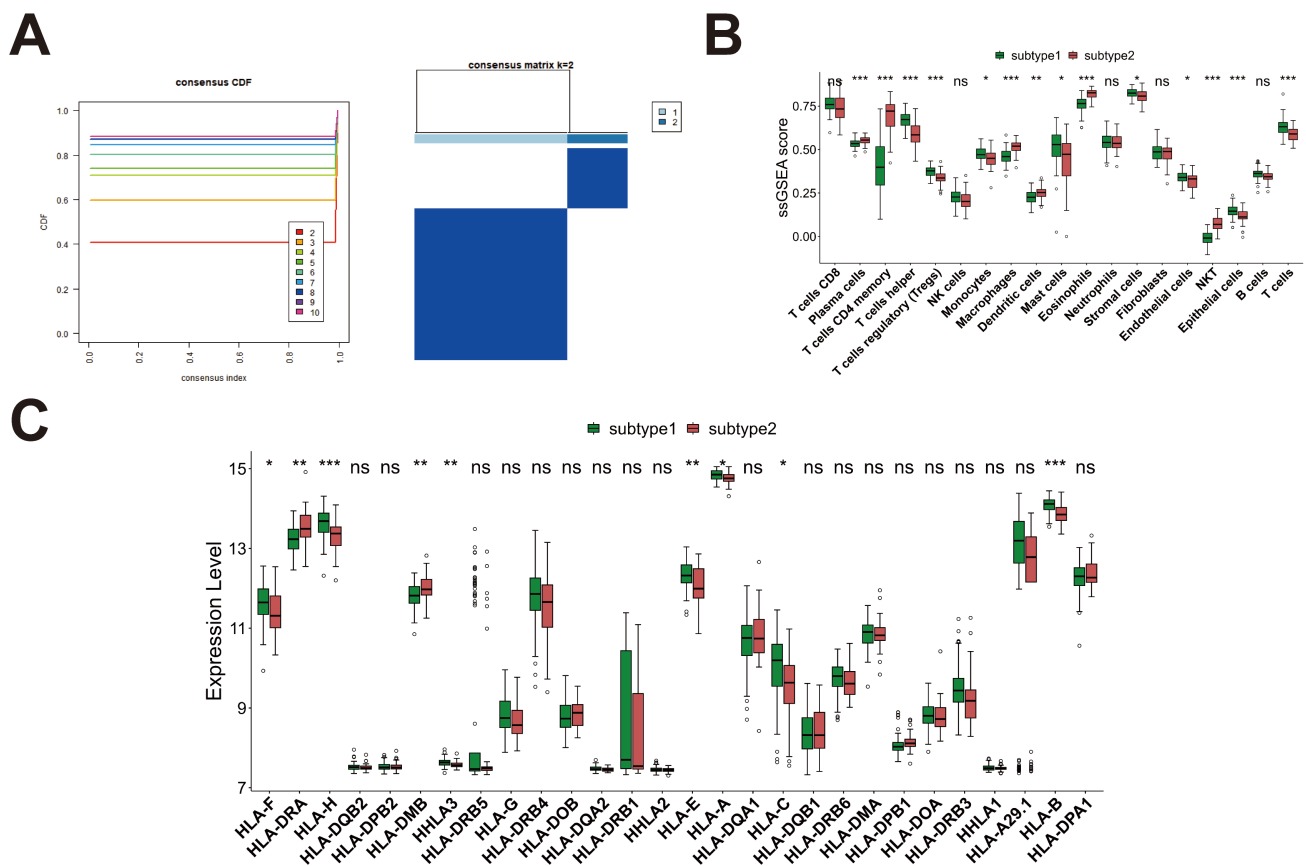


**Fig. 3. Subtype analysis.** (A) Subtype identification. Left panel: empirical cumulative distribution function (CDF) plot of consistency clustering for  $k = 2-10$ . Right panel: sample classification into two distinct subtypes (subtype 1 and subtype 2). (B) Differential immune cell infiltration between the two subtypes. (C) Comparison of HLA gene expression between the two groups. ns, not significant; \*,  $p < 0.05$ ; \*\*,  $p < 0.01$ ; \*\*\*,  $p < 0.001$ . NKT, natural killer cell; HLA, human leukocyte antigen; ss-GSEA, single-sample Gene Set Enrichment Analysis; DRA, HLA-Major Histocompatibility Complex Class II DR Alpha; DMB, HLA-Major Histocompatibility Complex Class II DM Beta.

### Discussion

The present study identified 149 genes associated with LLPS, which were implicated in oxidative stress, apoptosis, and cancer progression. Through subtype analysis, all AD samples were divided into subtype 1 and subtype 2, with higher immune infiltration in subtype 2. Furthermore, by using PPI and LASSO analyses, the 149 genes were optimized into six: *AHSA1*, *EIF2AK2*, *HSPA4*, *NOTCH1*, *SOD1*, and *TXN*. Based on the six optimal genes, a diagnostic risk model was constructed, and the diagnostic ability was verified to be promising in AD in training, internal validation, and external validation datasets. Finally, these genes were significantly correlated with immune cell infiltration.

Among the six genes involved in the diagnostic model, four have been implicated in the progression and patholog-

ical mechanisms of AD: *AHSA1*, *EIF2AK2*, *NOTCH1*, and *SOD1*. The Notch1 signaling pathway, crucial for brain development, exhibits overexpression in AD and may contribute to its pathophysiology [22]. Superoxide dismutase 1 (*SOD1*), an antioxidant enzyme, is associated with accelerated aging in neurodegenerative diseases [23,24]. *AHSA1*, an activator of heat shock protein 90 (Hsp90) ATPase, is upregulated in various tumors and has been shown to participate in various metabolic and development processes in tumor cells [25–27]. In AD, studies have demonstrated that *Aha1* is upregulated in the hippocampus of tau transgenic mice, potentially leading to increased levels of oligomeric and insoluble tau. This upregulation is associated with neuronal loss and cognitive impairments [28,29]. Inhibition of Aha1 has been proposed as a potential therapeutic strategy to mitigate the formation of toxic tau oligomers and prevent AD progression [28]. *EIF2AK2*, also known as double-stranded RNA-dependent protein kinase R (PKR),



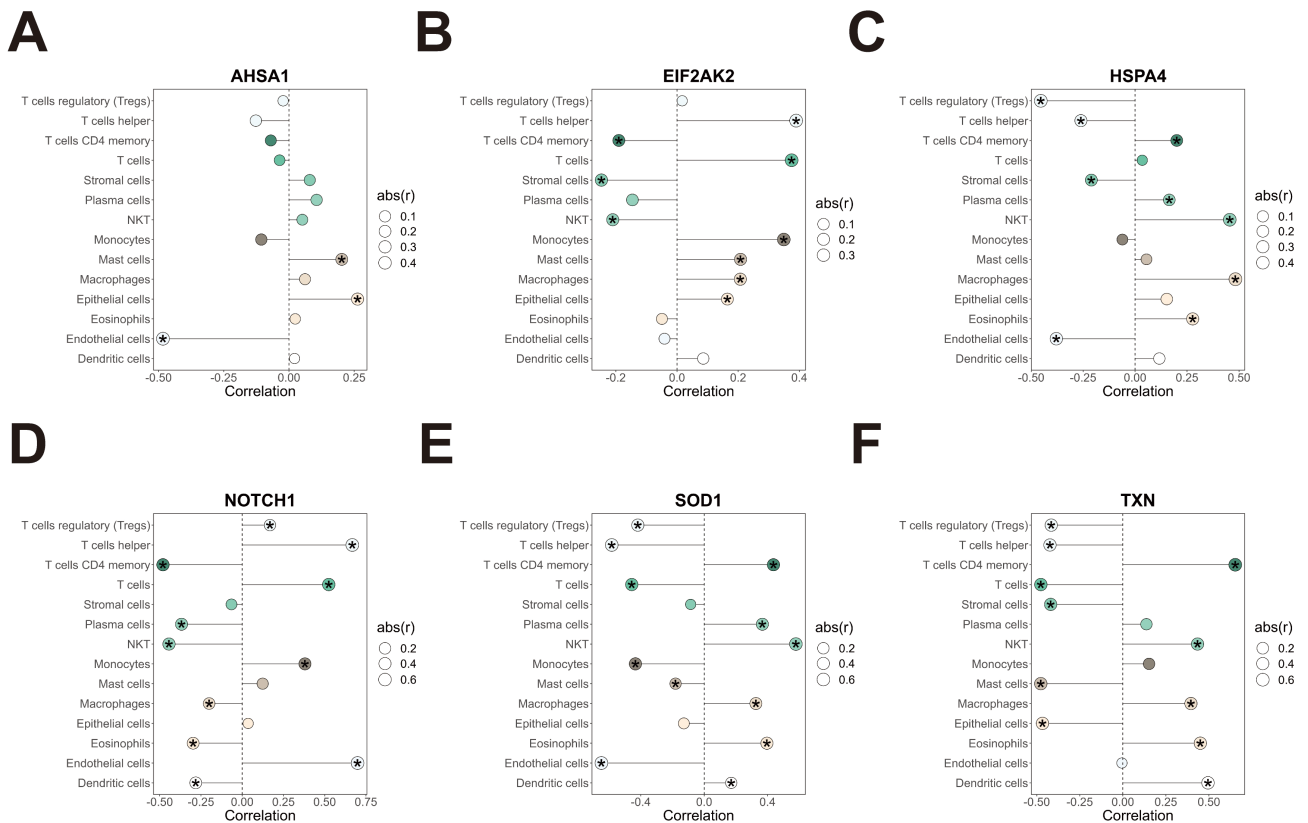


**Fig. 5. Correlation between optimal LLPS-related genes in the diagnostic model and immune cells.** (A) Correlation of Activator of HSP90 ATPase Activity 1 (*AHS1*) with immune cells. (B) Correlation of Eukaryotic Translation Initiation Factor 2 Alpha Kinase 2 (*EIF2AK2*) with immune cells. (C) Correlation of Heat Shock Protein Family A (Hsp70) Member 4 (*HSPA4*) with immune cells. (D) Correlation of Notch Receptor 1 (*NOTCH1*) with immune cells. (E) Correlation of Superoxide Dismutase 1 (*SOD1*) with immune cells. (F) Correlation of Thioredoxin (*TXN*) with immune cells. \* represents significance; right represents positive correlation; left represents negative correlation. LLPS, liquid-liquid phase separation.

in the pathogenesis of this neurodegenerative disorder [31]. Lopez-Grancha *et al.* [32] demonstrated that the inhibition of *EIF2AK2* ameliorates cognitive deficits and neurodegeneration in AD mouse models, as evidenced by restoration of synaptic proteins and reduction of proinflammatory cytokine levels. The roles of *HSPA4* and *TXN* in AD pathogenesis remain unclear. Two studies suggest that the *HSPA4* protein might be related to specific targets and pathways in AD [33,34], although the precise mechanisms remain unknown. *TXN* (thioredoxin) has been implicated in inflammatory, metabolic, and redox processes across various diseases [35–37].

The evidence presented suggests that the six genes in the diagnostic model may be closely associated with the progression and pathological mechanisms of AD, further supporting the robustness of the model. Nevertheless, several limitations should be acknowledged. First, the diagnosis model requires validation in larger-scale cohorts. Sec-

ond, further investigation is needed to fully elucidate the mechanisms of action for the six optimal genes, particularly *HSPA4* and *TXN*. Third, the correlation between the six key genes and LLPS remains unclear, necessitating additional research in this area. Finally, there is a current lack of targeted therapeutics based on these diagnostic biomarkers for AD. Despite these limitations, we have developed an optimal diagnostic model for AD with an AUC above 0.8. This study provides valuable insights for future research into the pathological mechanisms of AD and potential therapeutic targets.

**Conclusions**

A diagnostic risk model for AD has been developed incorporating six genes associated with LLPS. These genes are: *AHS1*, *EIF2AK2*, *HSPA4*, *NOTCH1*, *SOD1*, and *TXN*. The diagnostic efficacy of this model has been evalu-

ated across multiple datasets, demonstrating promising results in identifying AD. These findings suggest that LLPS-related genes may play a significant role in AD pathogenesis and could serve as potential biomarkers for early detection and diagnosis.

## Availability of Data and Materials

The datasets used and/or analyzed during the current study are available from the corresponding author on reasonable request.

## Author Contributions

Study conception and design: CQ, HX; data collection: CQ; analysis and interpretation of results: HX; draft manuscript preparation: CQ. Both authors reviewed the results. Both authors contributed to important editorial changes in the manuscript. Both authors read and approved the final manuscript. Both authors have participated sufficiently in the work and agreed to be accountable for all aspects of the work.

## Ethics Approval and Consent to Participate

Not applicable.

## Acknowledgment

Not applicable.

## Funding

This research received no funding.

## Conflict of Interest

The authors declare no conflict of interest.

## References

- [1] Ma X, Wang X, Xiao Y, Zhao Q. Retinal examination modalities in the early detection of Alzheimer's disease: Seeing brain through the eye. *Journal of Translational Internal Medicine*. 2022; 10: 185–187.
- [2] Yin Z, Wong S. Converging multi-modality datasets to build efficient drug repositioning pipelines against Alzheimer's disease and related dementias. *Medical Review*. 2022; 2: 110–113.
- [3] Scheltens P, De Strooper B, Kivipelto M, Holstege H, Chételat G, Teunissen CE, *et al.* Alzheimer's disease. *Lancet (London, England)*. 2021; 397: 1577–1590.
- [4] Song X, Mitnitski A, Rockwood K. Nontraditional risk factors combine to predict Alzheimer disease and dementia. *Neurology*. 2011; 77: 227–234.
- [5] Briggs R, Kennelly SP, O'Neill D. Drug treatments in Alzheimer's disease. *Clinical Medicine (London, England)*. 2016; 16: 247–253.
- [6] Gong B, Zhuang J, Ji W, Chen X, Li P, Cheng W, *et al.* The long and the short of current nanomedicines for treating Alzheimer's disease. *Journal of Translational Internal Medicine*. 2022; 10: 294–296.
- [7] Fu Q, Zhang B, Chen X, Chu L. Liquid-liquid phase separation in Alzheimer's disease. *Journal of Molecular Medicine (Berlin, Germany)*. 2024; 102: 167–181.
- [8] Liu B, Shen H, He J, Jin B, Tian Y, Li W, *et al.* Cytoskeleton remodeling mediated by circRNA-YBX1 phase separation suppresses the metastasis of liver cancer. *Proceedings of the National Academy of Sciences of the United States of America*. 2023; 120: e2220296120.
- [9] Boyko S, Surewicz WK. Tau liquid-liquid phase separation in neurodegenerative diseases. *Trends in Cell Biology*. 2022; 32: 611–623.
- [10] Wegmann S, Eftekharzadeh B, Tepper K, Zoltowska KM, Bennett RE, Dujardin S, *et al.* Tau protein liquid-liquid phase separation can initiate tau aggregation. *The EMBO Journal*. 2018; 37: e98049.
- [11] Boyko S, Surewicz K, Surewicz WK. Regulatory mechanisms of tau protein fibrillation under the conditions of liquid-liquid phase separation. *Proceedings of the National Academy of Sciences of the United States of America*. 2020; 117: 31882–31890.
- [12] Chatterjee P, Pedrini S, Ashton NJ, Tegg M, Goozee K, Singh AK, *et al.* Diagnostic and prognostic plasma biomarkers for preclinical Alzheimer's disease. *Alzheimer's & Dementia: the Journal of the Alzheimer's Association*. 2022; 18: 1141–1154.
- [13] He YJ, Cong L, Liang SL, Ma X, Tian JN, Li H, *et al.* Discovery and validation of Ferroptosis-related molecular patterns and immune characteristics in Alzheimer's disease. *Frontiers in Aging Neuroscience*. 2022; 14: 1056312.
- [14] Pei Y, Chen S, Zhou F, Xie T, Cao H. Construction and evaluation of Alzheimer's disease diagnostic prediction model based on genes involved in mitophagy. *Frontiers in Aging Neuroscience*. 2023; 15: 1146660.
- [15] Ritchie ME, Phipson B, Wu D, Hu Y, Law CW, Shi W, *et al.* limma powers differential expression analyses for RNA-sequencing and microarray studies. *Nucleic Acids Research*. 2015; 43: e47.
- [16] Ito K, Murphy D. Application of ggplot2 to Pharmacometric Graphics. *CPT: Pharmacometrics & Systems Pharmacology*. 2013; 2: e79.
- [17] Wu T, Hu E, Xu S, Chen M, Guo P, Dai Z, *et al.* clusterProfiler 4.0: A universal enrichment tool for interpreting omics data. *Innovation (Cambridge (Mass.))*. 2021; 2: 100141.
- [18] Wilkerson MD, Hayes DN. ConsensusClusterPlus: a class discovery tool with confidence assessments and item tracking. *Bioinformatics (Oxford, England)*. 2010; 26: 1572–1573.
- [19] Hänzelmann S, Castelo R, Guinney J. GSEA: gene set variation analysis for microarray and RNA-seq data. *BMC Bioinformatics*. 2013; 14: 7.
- [20] Szklarczyk D, Gable AL, Nastou KC, Lyon D, Kirsch R, Pyysalo S, *et al.* The STRING database in 2021: customizable protein-

- protein networks, and functional characterization of user-uploaded gene/measurement sets. *Nucleic Acids Research*. 2021; 49: D605–D612.
- [21] Engebretsen S, Bohlin J. Statistical predictions with glmnet. *Clinical Epigenetics*. 2019; 11: 123.
- [22] Brai E, Alina Raio N, Alberi L. Notch1 hallmarks fibrillary depositions in sporadic Alzheimer's disease. *Acta Neuropathologica Communications*. 2016; 4: 64.
- [23] Shafiq K, Sanghai N, Guo Y, Kong J. Implication of post-translationally modified SOD1 in pathological aging. *GeroScience*. 2021; 43: 507–515.
- [24] Bader JM, Geyer PE, Müller JB, Strauss MT, Koch M, Leyboldt F, *et al.* Proteome profiling in cerebrospinal fluid reveals novel biomarkers of Alzheimer's disease. *Molecular Systems Biology*. 2020; 16: e9356.
- [25] Li W, Liu J. The Prognostic and Immunotherapeutic Significance of AHSA1 in Pan-Cancer, and Its Relationship with the Proliferation and Metastasis of Hepatocellular Carcinoma. *Frontiers in Immunology*. 2022; 13: 845585.
- [26] Gu C, Wang Y, Zhang L, Qiao L, Sun S, Shao M, *et al.* AHSA1 is a promising therapeutic target for cellular proliferation and proteasome inhibitor resistance in multiple myeloma. *Journal of Experimental & Clinical Cancer Research: CR*. 2022; 41: 11.
- [27] Shao J, Wang L, Zhong C, Qi R, Li Y. AHSA1 regulates proliferation, apoptosis, migration, and invasion of osteosarcoma. *Biomedicine & Pharmacotherapy = Biomedecine & Pharmacotherapie*. 2016; 77: 45–51.
- [28] Shelton LB, Baker JD, Zheng D, Sullivan LE, Solanki PK, Webster JM, *et al.* Hsp90 activator Aha1 drives production of pathological tau aggregates. *Proceedings of the National Academy of Sciences of the United States of America*. 2017; 114: 9707–9712.
- [29] Criado-Marrero M, Gebru NT, Blazier DM, Gould LA, Baker JD, Beaulieu-Abdelahad D, *et al.* Hsp90 co-chaperones, FKBP52 and Aha1, promote tau pathogenesis in aged wild-type mice. *Acta Neuropathologica Communications*. 2021; 9: 65.
- [30] Bullido MJ, Martínez-García A, Tenorio R, Sastre I, Muñoz DG, Frank A, *et al.* Double stranded RNA activated EIF2 alpha kinase (EIF2AK2; PKR) is associated with Alzheimer's disease. *Neurobiology of Aging*. 2008; 29: 1160–1166.
- [31] Heneka MT, Kummer MP, Stutz A, Delekate A, Schwartz S, Vieira-Saecker A, *et al.* NLRP3 is activated in Alzheimer's disease and contributes to pathology in APP/PS1 mice. *Nature*. 2013; 493: 674–678.
- [32] Lopez-Grancha M, Bernardelli P, Moindrot N, Genet E, Vincent C, Roudieres V, *et al.* A Novel Selective PKR Inhibitor Restores Cognitive Deficits and Neurodegeneration in Alzheimer Disease Experimental Models. *The Journal of Pharmacology and Experimental Therapeutics*. 2021; 378: 262–275.
- [33] Mao Y, Fisher DW, Yang S, Keszycki RM, Dong H. Protein-protein interactions underlying the behavioral and psychological symptoms of dementia (BPSD) and Alzheimer's disease. *PLoS One*. 2020; 15: e0226021.
- [34] Qian XH, Liu XL, Chen SD, Tang HD. Identification of Immune Hub Genes Associated with Braak Stages in Alzheimer's Disease and Their Correlation of Immune Infiltration. *Frontiers in Aging Neuroscience*. 2022; 14: 887168.
- [35] Ball DP, Tsamouri LP, Wang AE, Huang HC, Warren CD, Wang Q, *et al.* Oxidized thioredoxin-1 restrains the NLRP1 inflammasome. *Science Immunology*. 2022; 7: eabm7200.
- [36] Espinosa B, Arnér ESJ. Thioredoxin-related protein of 14 kDa as a modulator of redox signalling pathways. *British Journal of Pharmacology*. 2019; 176: 544–553.
- [37] Zhang J, Li X, Han X, Liu R, Fang J. Targeting the Thioredoxin System for Cancer Therapy. *Trends in Pharmacological Sciences*. 2017; 38: 794–808.